

Generating Experimental Data for a Three-Dimensional Generalized Composite Material Model

Bilal Khaled, Nathan Holt, Loukham Shyamsunder, Canio Hoffarth and Subramaniam D. Rajan
School of Sustainable Engineering and the Built Environment, Arizona State University, Tempe, AZ

Robert K. Goldberg

NASA-GRC, Cleveland, OH

Kelly S. Carney and Paul DuBois

George Mason University, Fairfax, VA

Gunther Blankenhorn

LSTC, Livermore, CA

Abstract

A three-dimensional orthotropic elasto-plastic composite material model is being implemented in a special version of LS-DYNA® as MAT213. The model is driven by experimental data that describe the elasto-plastic deformation behavior, coupled and uncoupled damage, and failure. This paper documents the test procedures to characterize the material behavior via tensile, compressive, shear and off-axis tests of as well as tests to generate validation data via stacked ply coupons. The theory and implementation of the algorithm are discussed in companion papers. A unidirectional composite, T800-F3900 fiber/resin composite material, commonly used in the aerospace industry is used to illustrate experimental procedures followed by the verification and validation processes.

Introduction

MAT 213 is a tabulated orthotropic elasto plastic damage three-dimensional finite element material model being developed through a sponsored research project funded by the FAA and NASA. Three distinct modules, deformation, damage, and failure, comprise the material model. The theoretical details of the three modules have been documented in previous publications (Goldberg et al., 2015; Goldberg et al., 2017; Hoffarth et al., 2016; Hoffarth et al., 2017). All components of MAT 213 are driven entirely by tabulated experimental data. The deformation model is driven by stress-strain curves and their derived parameters and allows for data corresponding to various strain rates and temperatures (Harrington et al., 2017). The damage model is driven by data obtained through cyclic testing. The failure model allows for a general tabulated failure surface in either stress or strain space and the necessary data can be obtained by performing experiments under various stress or strain combinations. In order to ensure accuracy of the material model, reliable experimental methods have been developed in order to generate the necessary experimental data. In this paper, we present the experimental methods used to obtain quasistatic and room temperature (QS-RT) monotonic stress-strain curves to drive the deformation model and QS-RT damage data for the T800/F3900 carbon fiber/epoxy resin unidirectional composite. Additionally, an open-hole tension test is presented which can be used as a validation test.

Constitutive Model Background

Deformation Model

In MAT 213, the linear and nonlinear deformation is handled with a plasticity formulation using a non-associative flow rule. A quadratic yield function is used which takes the form of the Tsai-Wu failure criteria shown in Equation 1.

$$f(\sigma) = a + (F_1 \ F_2 \ F_3 \ 0 \ 0 \ 0) \begin{bmatrix} \sigma_{11} \\ \sigma_{22} \\ \sigma_{33} \\ \sigma_{12} \\ \sigma_{23} \\ \sigma_{31} \end{bmatrix} + \begin{bmatrix} \sigma_{11} \\ \sigma_{22} \\ \sigma_{33} \\ \sigma_{12} \\ \sigma_{23} \\ \sigma_{31} \end{bmatrix}^T \begin{bmatrix} F_{11} & F_{12} & F_{13} & 0 & 0 & 0 \\ F_{12} & F_{22} & F_{23} & 0 & 0 & 0 \\ F_{13} & F_{23} & F_{33} & 0 & 0 & 0 \\ 0 & 0 & 0 & F_{44} & 0 & 0 \\ 0 & 0 & 0 & 0 & F_{55} & 0 \\ 0 & 0 & 0 & 0 & 0 & F_{66} \end{bmatrix} \begin{bmatrix} \sigma_{11} \\ \sigma_{22} \\ \sigma_{33} \\ \sigma_{12} \\ \sigma_{23} \\ \sigma_{31} \end{bmatrix} \quad (1)$$

where $a = -1$ and the yield function coefficients, F_{ij} , are functions of the current yield stresses (flow stresses). The values of the yield function coefficients are tracked using tabulated stress-strain curves as a function of the current effective plastic strain (Goldberg et al., 2015). The plastic potential function used in the non-associative flow rule is given by Equation 2.

$$h = \sqrt{H_{11}\sigma_{11}^2 + H_{22}\sigma_{22}^2 + H_{33}\sigma_{33}^2 + 2H_{12}\sigma_{11}\sigma_{22} + 2H_{23}\sigma_{22}\sigma_{33} + 2H_{31}\sigma_{33}\sigma_{11} + H_{44}\sigma_{12}^2 + H_{55}\sigma_{23}^2 + H_{66}\sigma_{31}^2} \quad (2)$$

where H_{ij} are referred to as flow rule coefficients and can be obtained from experimental data (Hoffarth et al., 2017). Both the yield function coefficients and the flow rule coefficients can be obtained by performing a series of physically meaningful, coupon level experiments. Though the plastic potential inherently does not account for tension/compression asymmetry due to the purely quadratic nature, the yield function allows for asymmetric behavior evidenced by the linear terms. Thus, the minimum input required to drive the deformation model is obtained from the following experiments under QS-RT conditions: tension and compression in the three principal material directions (PMD), shear in the three principal planes, and off-axis tension or compression in the three principal material planes. The off-axis data aids in computing the interaction terms in the yield function. The flow rule coefficients can be computed using the plastic Poisson's ratios derived from the PMD tension and compression tests.

Damage Model

In the context of MAT 213, the deformation and damage models are decoupled from another which allows for all nonlinear behavior to be captured by the plasticity formulation. The damage model serves to capture the reduction in elastic stiffness which manifests due to several phenomena at the microscale. Decoupling of the deformation and damage models is achieved by assuming a strain equivalence and defining the effective and true stress spaces. A damage tensor shown in Equation 3 is used to relate the two stress spaces.

$$\begin{pmatrix} \sigma_{11} \\ \sigma_{22} \\ \sigma_{33} \\ \sigma_{12} \\ \sigma_{23} \\ \sigma_{13} \end{pmatrix} = \begin{bmatrix} M_{11} & M_{12} & M_{13} & M_{14} & M_{15} & M_{16} \\ M_{21} & M_{22} & M_{23} & M_{24} & M_{25} & M_{26} \\ M_{31} & M_{32} & M_{33} & M_{34} & M_{35} & M_{36} \\ M_{41} & M_{42} & M_{43} & M_{44} & M_{45} & M_{46} \\ M_{51} & M_{52} & M_{53} & M_{54} & M_{55} & M_{56} \\ M_{61} & M_{62} & M_{63} & M_{64} & M_{65} & M_{66} \end{bmatrix} \begin{pmatrix} \sigma_{11}^{eff} \\ \sigma_{22}^{eff} \\ \sigma_{33}^{eff} \\ \sigma_{12}^{eff} \\ \sigma_{23}^{eff} \\ \sigma_{13}^{eff} \end{pmatrix} \quad (3)$$

However, in our damage model implementation, the damage model assumes a semi-coupled, directional dependent relationship given by

$$\begin{pmatrix} \sigma_{11} \\ \sigma_{22} \\ \sigma_{33} \\ \sigma_{12} \\ \sigma_{23} \\ \sigma_{13} \end{pmatrix} = \begin{bmatrix} M_{11} & 0 & 0 & 0 & 0 & 0 \\ 0 & M_{22} & 0 & 0 & 0 & 0 \\ 0 & 0 & M_{33} & 0 & 0 & 0 \\ 0 & 0 & 0 & M_{44} & 0 & 0 \\ 0 & 0 & 0 & 0 & M_{55} & 0 \\ 0 & 0 & 0 & 0 & 0 & M_{66} \end{bmatrix} \begin{pmatrix} \sigma_{11}^{eff} \\ \sigma_{22}^{eff} \\ \sigma_{33}^{eff} \\ \sigma_{12}^{eff} \\ \sigma_{23}^{eff} \\ \sigma_{13}^{eff} \end{pmatrix} \quad (4)$$

where M_{ii} is a damage term which is a function of all directions, i.e. $M_{22} = M_{22}(\varepsilon_p^{11}, \varepsilon_p^{22}, \varepsilon_p^{33}, \varepsilon_p^{12}, \varepsilon_p^{23}, \varepsilon_p^{13})$. The damage terms consist of a multiplicative series of damage parameters defined as, d_{ij}^{kl} , representing damage in direction kl due to loading along direction ij , and are tracked as a function of directional plastic strain. The definition of the damage parameter indicates that both uncoupled and coupled damage may be captured by the model. The damage model allows for asymmetric damage caused by either tensile or compressive stresses. An example of one of the components of the damage tensor is shown in Equation 5. Equation 5 also shows that coupling between normal and shear directions is accounted for.

$$M_{22} = \begin{cases} \text{if } \sigma_{22} \geq 0 \rightarrow (1 - d_{11r}^{22r}(\varepsilon_{11r}^p))(1 - d_{11c}^{22r}(\varepsilon_{11c}^p))(1 - d_{22r}^{22r}(\varepsilon_{22r}^p))(1 - d_{22c}^{22r}(\varepsilon_{22c}^p))(1 - d_{33r}^{22r}(\varepsilon_{33r}^p))(1 - d_{33c}^{22r}(\varepsilon_{33c}^p))(1 - d_{12}^{22r}(\varepsilon_{12}^p))(1 - d_{23}^{22r}(\varepsilon_{23}^p))(1 - d_{13}^{22r}(\varepsilon_{13}^p)) \\ \text{if } \sigma_{22} < 0 \rightarrow (1 - d_{11r}^{22c}(\varepsilon_{11r}^p))(1 - d_{11c}^{22c}(\varepsilon_{11c}^p))(1 - d_{22r}^{22c}(\varepsilon_{22r}^p))(1 - d_{22c}^{22c}(\varepsilon_{22c}^p))(1 - d_{33r}^{22c}(\varepsilon_{33r}^p))(1 - d_{33c}^{22c}(\varepsilon_{33c}^p))(1 - d_{12}^{22c}(\varepsilon_{12}^p))(1 - d_{23}^{22c}(\varepsilon_{23}^p))(1 - d_{13}^{22c}(\varepsilon_{13}^p)) \end{cases} \quad (5)$$

Allowing for full coupling and tension/compression asymmetry leads to a total of 84 damage parameters that may be obtained experimentally. The general form of the damage parameters is shown in Equation 6.

$$d_{ij}^{kl} = 1 - \frac{E_{kl}^d(\varepsilon_{ij}^p)}{E_{kl}} \quad (6)$$

The damage parameters can be obtained experimentally through a series of loading/unloading tests. The damage is tracked as a function of directional plastic strain using tabulated input rather than using an analytical damage evolution law.

Failure Model

Failure is handled independently from damage in the context of MAT 213. A tabulated failure surface approach has been developed and presented in another publication (Goldberg et al., 2017). The failure model handles both in-plane and out-of-plane failure of the material and the combination of the two. Either stress or strain data may be used to generate the tabulated failure surface. Additional details of how the experimental data is generated will be presented in an upcoming publication (Shyamsunder et al., 2018b).

Experimental Methods and Results

Generating experimental data to drive any material model requires the development of proper experimental techniques which can be used to reliably capture the behavior of the material in question. The term “experimental techniques” encompasses specimen preparation, testing procedures, and post processing of experimental data. This section presents the experimental techniques and results for the tests used to characterize the nonlinear deformation behavior and damage behavior of the T800/F3900 unidirectional carbon fiber/epoxy resin composite system, manufactured by Toray (2017). Additionally, QS-RT cross-ply tests were conducted and are used to validate the deformation and failure models in MAT 213. The experimental techniques are the same for all tests unless otherwise noted.

Specimen Preparation

The T800/F3900 composite was used to generate the required experimental data to drive the deformation, damage, and failure models. Toray composites provided three different composite panel types: 16 plies (3.1 mm), 24 plies (4.7 mm), and 96 plies (18.3 mm). A waterjet was used to generate the necessary test coupons. Details of the waterjet specifications and the panels used to cut each specimen are outlined in Khaled et al., 2017. For the QS-RT monotonic and damage tests, the panels were made up of plies with the same orientation, i.e. $[0]_n$. Additionally, G10 fiberglass tabs were used with tension and shear tests to provide a compliant surface which prevents crushing during testing.

Experimental Equipment

All experiments were performed using an MTS 810 servo hydraulic test frame. Figure 1 shows various fixtures used in performing specific tests. All tests were conducted under crosshead displacement control with a rate in accordance with the corresponding ASTM. The experimental results presented herein correspond to room temperature and quasi-static conditions (strain rate in the range $10^{-4} / s - 10^{-3} / s$).

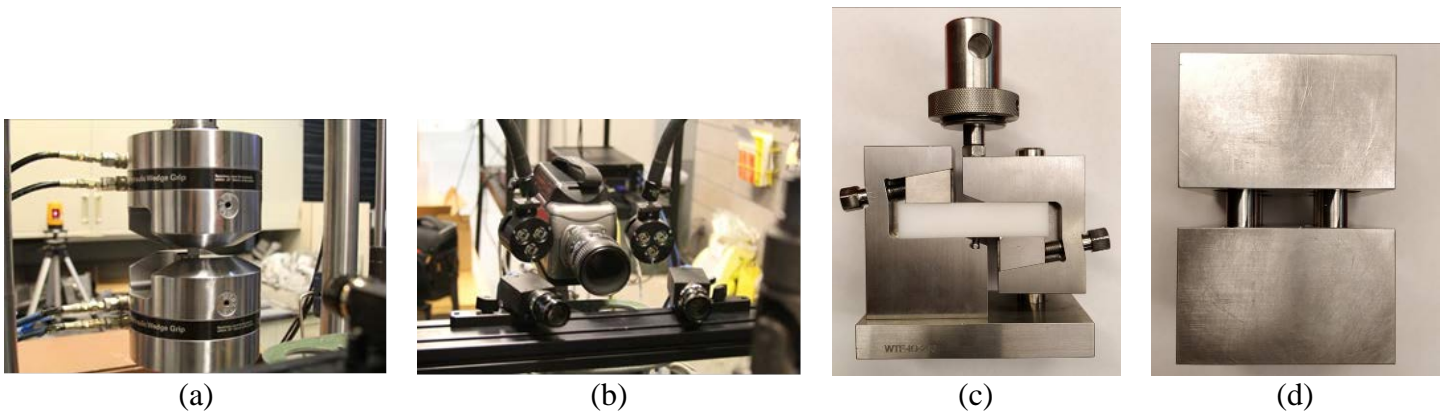


Figure 1. (a) Hydraulic grips for tension tests, (b) DIC equipment, (c) Iosipescu shear test fixture, and (d) Combined loading compression fixture

Digital image correlation (DIC) was used to compute full field strain fields and subsequently construct stress-strain curves for all experiments conducted for this research. Vic-3d (Correlated Solutions Inc., 2017) was used to perform the image analysis. Figure 2 shows a typical speckled surface and resulting strain field obtained DIC at one instance during the experimental procedure.

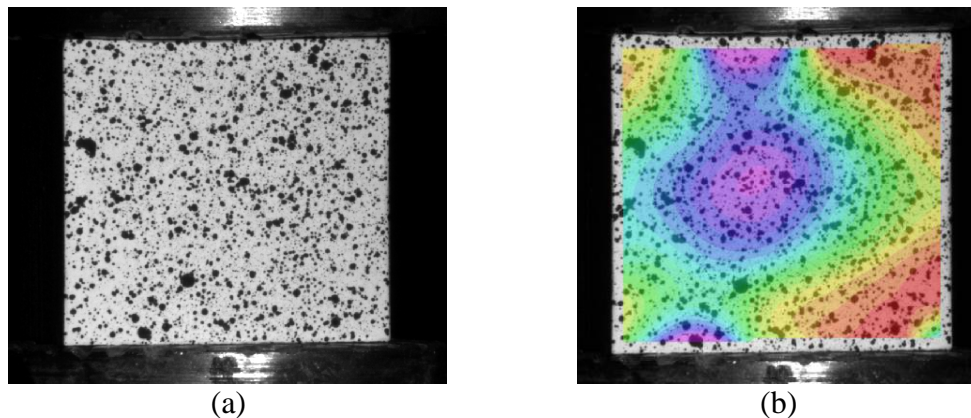


Figure 2. 3-direction compression test (a) Speckled specimen and (b) Resulting longitudinal strain field.

Post Processing of Experimental Data

After performing multiple replicates of each experiment, each yielding consistent and reliable data, a single model curve is generated which serves as the representative material behavior used to drive the deterministic material model. The model curve is a point-by-point average of the replicate curves. The deformation model is driven by the stress-total strain curves whereas the damage model is driven by damage parameter–total strain curves.

QS-RT Experiments

QS-RT tests to obtain the data required to drive the deformation model used a monotonic loading procedure. Each of the twelve required experiments were successfully performed and yielded consistent data. While the tension and compression tests were loaded to a clear, discernable point of failure, the shear tests exhibited ambiguous failure data.

A few observations can be made regarding the material behavior that affect the deformation model. The first is that a clear asymmetry was observed in the tension and compression response of the principal material directions. The model curves for the respective 1-direction tests are shown in Figure 3.

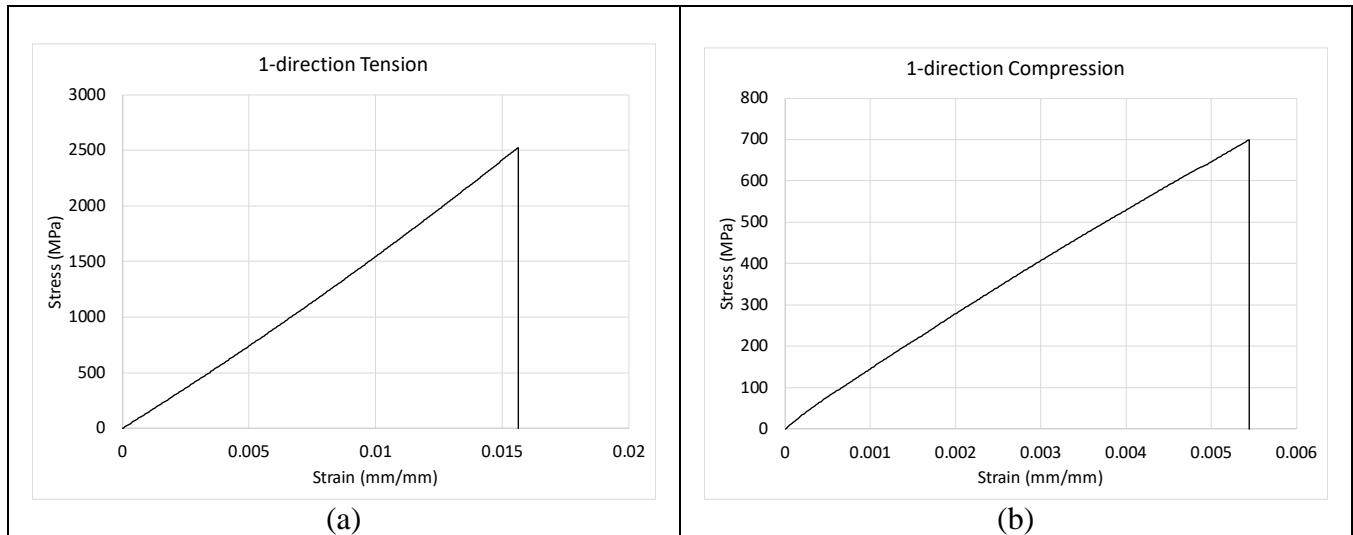


Figure 3. 1-direction model curves (a) tension response and (b) compression response

The principal material directions generally exhibited vastly different responses in tension and compression. In the transverse directions, the compression data exhibited much greater nonlinear behavior than the tension data. In the longitudinal (fiber) direction, exhibited much higher strength in tension than in compression. The asymmetry in the experimental data causes difficulties in properly defining the plastic potential function because of its purely quadratic nature.

As previously mentioned, while the PMD tension and compression tests exhibited clear failure, the shear tests typically did not fail in a clear manner. This is likely due to high degree of anisotropy between the longitudinal and transverse directions. The ratio of elastic stiffness is approximately 20:1 while the ratio of tensile strength is approximately 65:1. These factors attribute to large deformations being experienced by the shear test specimens in the 1-2 and 1-3 planes. Figure 4 shows the stress-strain curves for both the 1-2 and 1-3 plane shear tests.

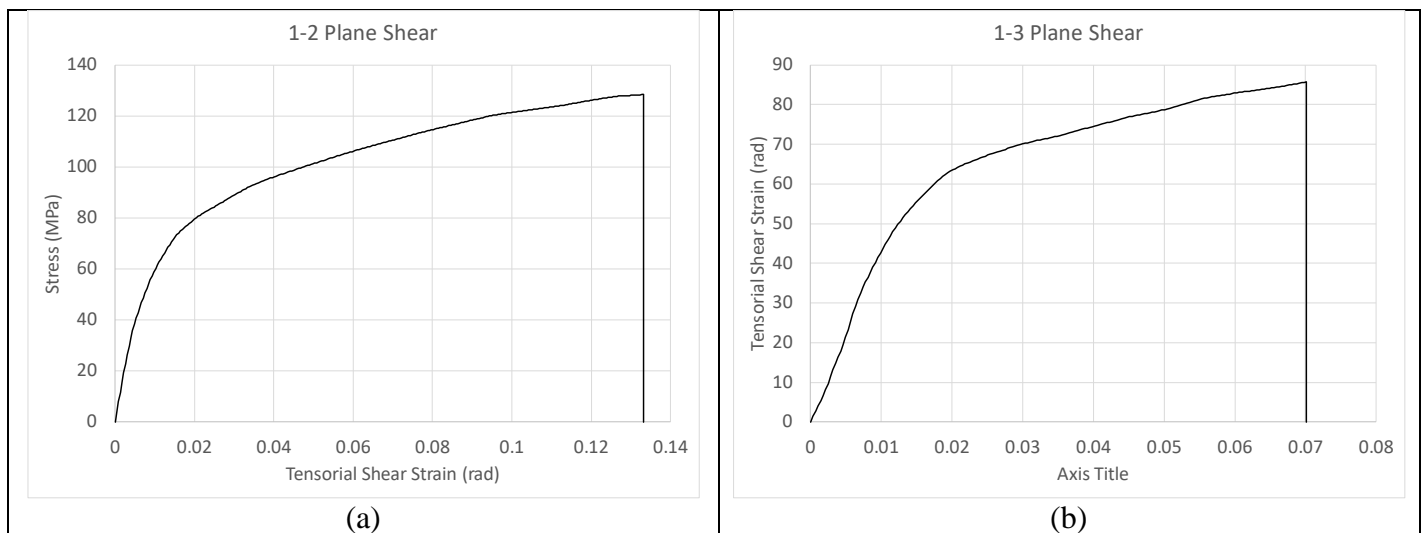


Figure 4. Model stress-strain curve (a) 1-2 plane shear test and (b) 1-3 plane shear test

In both the 1-2 and 1-3 plane test specimens, rather than failing in a brittle manner, begin to significantly crack near the root of the notch tips caused by the stresses exceeding the tensile strength in the transverse directions. However, even though the cracks become large, the specimens retain load carrying capacity. This phenomenon causes difficulties in defining the stress corresponding to failure in the material. Figure 5 shows typical 1-2 and 1-3 plane shear test specimens near the end of the testing procedure.

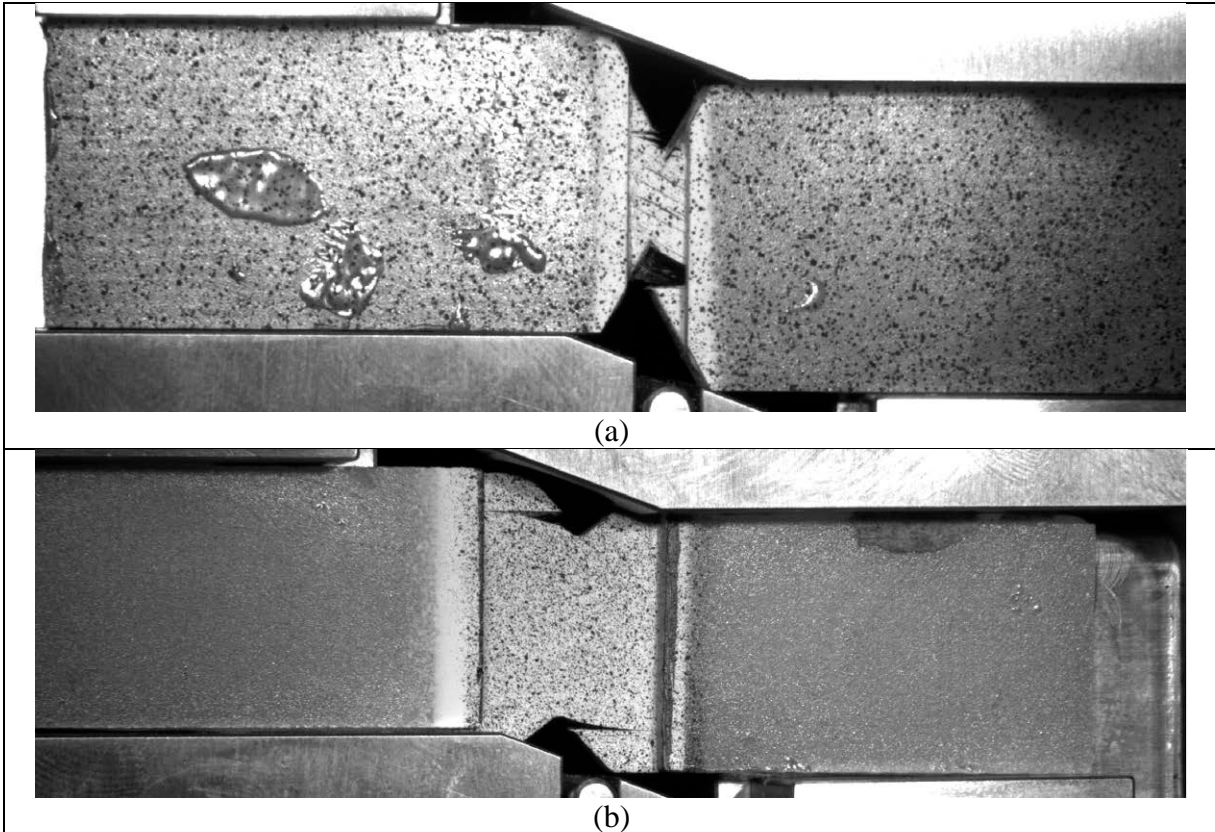


Figure 5. Failed Iosipescu shear test specimens (a) 1-2 plane and (b) 1-3 plane

The results obtained from all twelve QS-RT experiments have been documented and discussed in detail in a recent publication (Khaled et al., 2017a).

Damage Characterization Experiments

Driving the damage model requires the use of experimentally obtained damage parameter-total strain curves as input. The input allows for updating values of damage as a function of the plastic strain induced in the material. In the context of this research, damage is defined as the reduction of elastic stiffness when compared to the undamaged specimen. As such, cyclic loading experiments are required to characterize the desired material behavior. Two terms can be defined:

1. Loading direction: the principal material direction or plane which is being loaded in order to induce damage in the specimen.
2. Interrogation direction: the principal material direction or plane in which the stiffness reduction is being computed.

In an uncoupled test, the loading and interrogation directions are the same, in a coupled test the loading and interrogation directions are different. Both the uncoupled damage tests and the coupled damage tests use similar procedures. The testing procedure is as follows.

1. Load and unload the specimen elastically in the interrogation direction to obtain an initial estimate of the elastic stiffness
2. In the loading direction, load the specimen into the nonlinear regime up to a predetermined value of strain
3. Unload the specimen to a state of zero stress.
4. Load the specimen in the interrogation direction into the elastic regime.
5. Unload the specimen to a point of zero stress.
6. Load the specimen to a higher point of strain than in (2) in the loading direction.
7. Repeat process until desired number of cycles is completed.

Figure 6 shows an illustration of the test procedure for both coupled and uncoupled damage parameters.

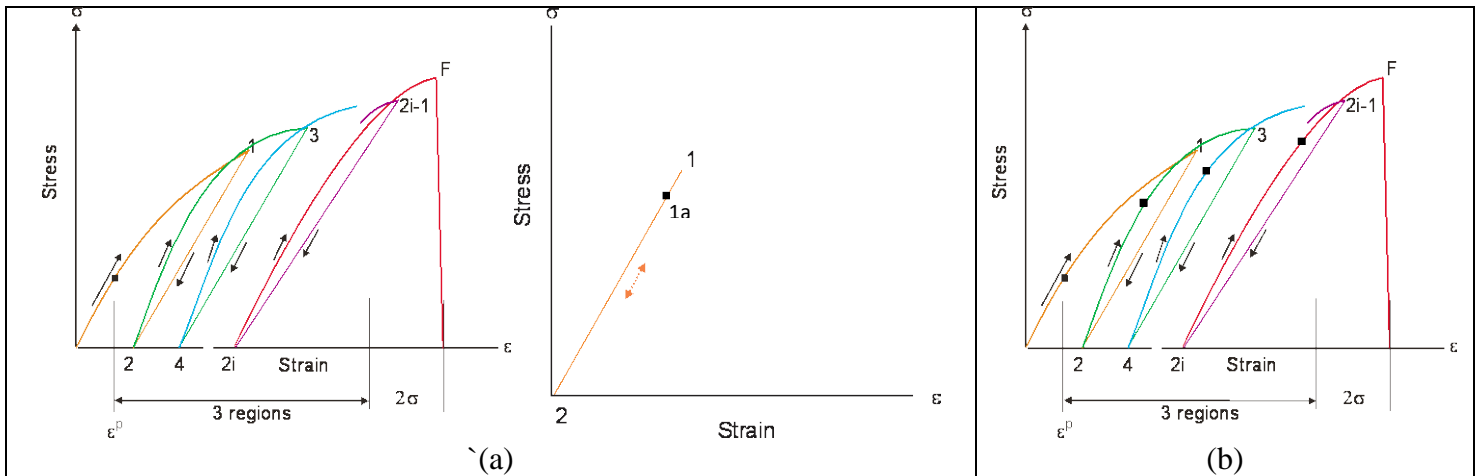


Figure 6. Damage characterization testing procedure (a) Coupled damage procedure and (b) Uncoupled damage procedure

Of the 84 possible experiments required to fully characterize the damage behavior of the material, four have been identified as being important in the context of this research: uncoupled 2-direction compression ($d_{22_c}^{22_c}$), uncoupled 1-2 plane shear (d_{12}^{12}), coupled 2-direction compression 2-direction tension ($d_{22_c}^{22_r}$), coupled 2-direction compression 1-2 plane shear ($d_{22_c}^{12}$). All four experiments correspond to in-plane damage properties of the composite. Both uncoupled and coupled damage has been observed in the results of the experiments. Figure 7 shows a sample damage parameter-total strain curve.

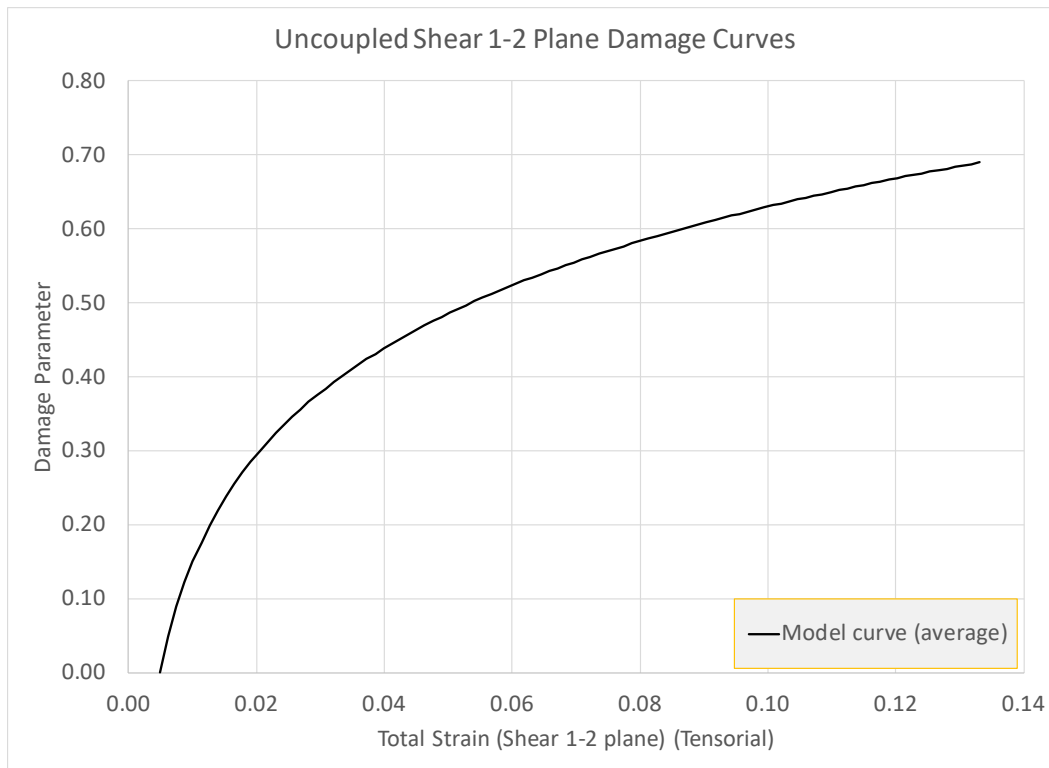


Figure 7. Uncoupled 1-2 plane shear model damage curve (d_{12}^{12})

The setup, procedure, and results of the damage characterization tests will be discussed in detail in an upcoming publication (Khaled et al., 2018).

QS-RT Validation Experiments

The QS-RT validation experiments will be used to validate the deformation and failure models. A $[0/90/+45/-45]_s$ layup was used to conduct four experiments: tension, compression, open-hole tension, and open-hole compression. The data obtained from these experiments is used only to validate not drive the material model. The model will be compared against the experimental data both qualitatively, with the DIC data, and quantitatively. Stress-strain curves from the DIC and load data will be compared to element stress-strain curves from the simulation. The open-hole tests will also be validated by comparing strain-rate curves from DIC data near the hole to element strain-rate curves from the simulation. Figure 8 shows a typical open-hole tension specimen after testing.

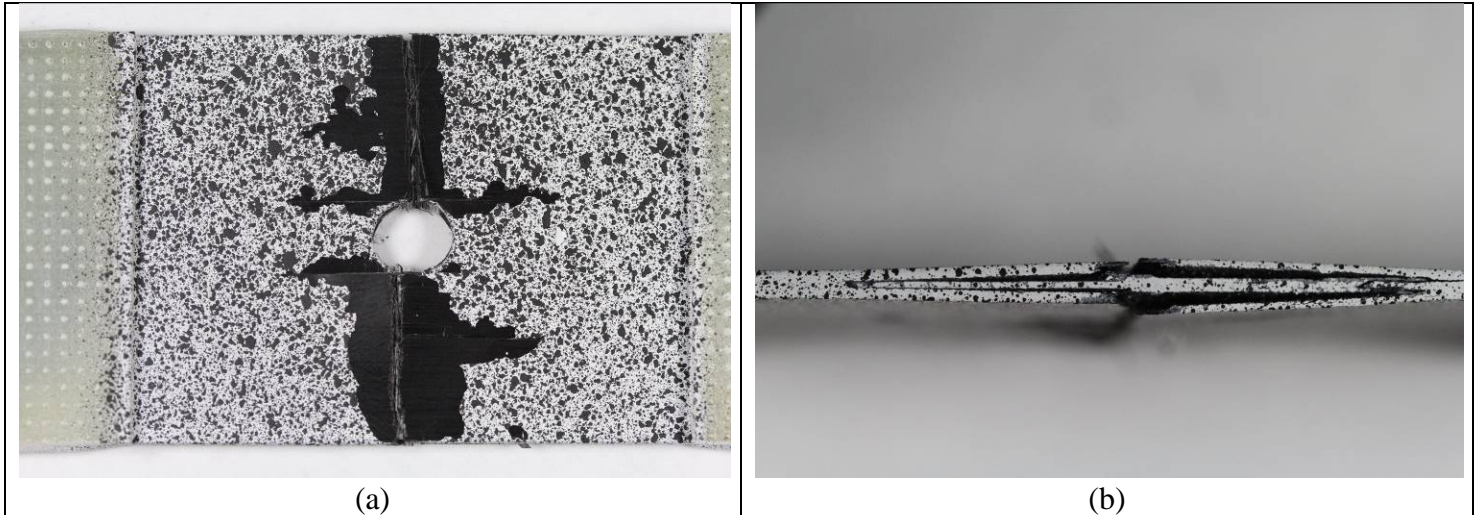


Figure 8. Failed open-hole tension experimental specimen (a) front view and (b) side view

Figure 9 shows the longitudinal strain field from a typical open-hole tension test. Note the strain concentrations present around the hole which is one of the motivators for performing this experiment.

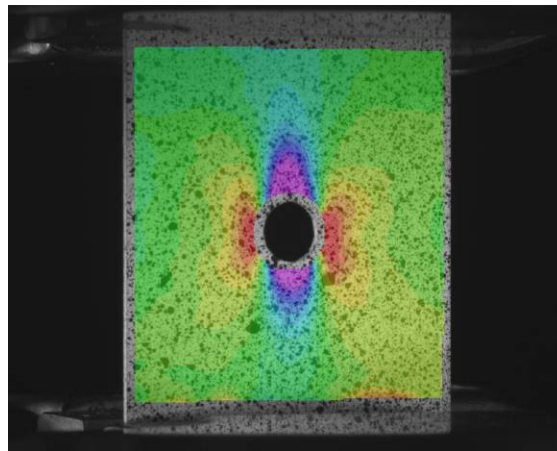


Figure 9. Open-hole tension longitudinal strain field

The full suite of experimental data will be fully presented in an upcoming publication (Shyamsunder et al., 2018b). Additional experiments, with increased complexity, will be conducted to validate the model. Part of the additional test suite is discussed in a companion paper as a part of this conference (Shyamsunder et al., 2018a).

Conclusions

In this paper, development of a new elasto-plastic-damage orthotropic constitutive material model has been discussed. The theoretical details are presented briefly to give background into which experiments need to be performed to drive the model. The general experimental methods needed to characterize an orthotropic material are presented and the results of a case study using the T800/F3900 composite are presented for the deformation, damage, and failure models.

Acknowledgements

Authors Khaled, Holt, Shyamsunder, Hoffarth, and Rajan gratefully acknowledge the support of (a) the Federal Aviation Administration through Grant #12-G-001 titled “Composite Material Model for Impact Analysis”, William Emmerling, Technical Monitor, and (b) NASA through Contract Number: NN15CA32C titled “Development and Implementation of an Orthotropic Plasticity Progressive Damage Model for Transient Dynamic/Impact Finite Element Analysis of Composite Structures”, Robert Goldberg, Contracting Officer Representative.

References

Correlated Solutions Inc. (2017). <http://correlatedsolutions.com/vic-3d/>

Goldberg, R., Carney, K., DuBois, P., Hoffarth, C., Harrington, J., Rajan, S., & Blankenhorn, G. (2015). Development of an Orthotropic Elasto-Plastic Generalized Composite Material Model Suitable for Impact Problems. *ASCE J of Aerospace Engineering*, 29(4).

Goldberg, R., Carney, K., DuBois, P., Hoffarth, C., Khaled, B., Shyamsunder, L., Rajan, S.D. and Blankenhorn, G. (2017). “Implementation of a Tabulated Failure Model into a Generalized Composite Material Model Suitable for Use in Impact problems”, American Society for Composites, Thirty-Second Technical Conference, 2017, Purdue University, West Lafayette, Indiana, USA.

Harrington, J., Hoffarth, C., Rajan, S.D., Goldberg, R., Carney, K., DuBois, P. and Blankenhorn, G. (2017). Using Virtual Tests to Complete the Description of a Three-Dimensional Orthotropic Material, *ASCE J of Aerospace Engineering*, DOI: 10.1061/(ASCE)AS.1943-5525.0000737.

Hoffarth, C., Rajan, S. D., Goldberg, R. K., Revilock, D., Carney, K. S., DuBois, P., & Blankenhorn, G. (2016). Implementation and validation of a three-dimensional plasticity-based deformation model for orthotropic composites. *Composites Part A: Applied Science and Manufacturing*, 91(1), 336-350.

Hoffarth, C., Khaled, B., Shyamsunder, L., Rajan, S. D., Goldberg, R. K., Carney, K. S., DuBois, P., & Blankenhorn, G. (2017). Verification and Validation of a Three-Dimensional Orthotropic Plasticity Constitutive Model Using a Unidirectional Composite. *Fibers*, 5(1), 1-13.

Khaled, B., Shyamsunder, L., Hoffarth, C., Rajan, S.D., Goldberg, R. K., Carney, K.S., DuBois, P., & Blankenhorn, G. (2017). Experimental Characterization of Composites to Support an Orthotropic Plasticity Material Model, *J of Composite Materials*, DOI: 10.1177/0021998317733319, August 2017.

Khaled, B., Shyamsunder, L., Hoffarth, C., Rajan, S.D., Goldberg, R. K., Carney, K.S., DuBois, P., & Blankenhorn, G. (2018). Damage Characterization of Composites to Support an Orthotropic Plasticity Material Model, under preparation.

LSTC (2017). LS-DYNA R8, <http://lsc.com/products/ls-dyna>

Shyamsunder, L., Khaled, B., Hoffarth, C., Rajan, S.D., Goldberg, R. K., Carney, K.S., DuBois, P., & Blankenhorn, G. (2018a). Using MAT213 for Simulation of High-Speed Impacts of Composite Structures, 15th International LS-DYNA Users Conference, Dearborn, MI

Shyamsunder, L., Khaled, B., Hoffarth, C., Rajan, S.D., Goldberg, R. K., Carney, K.S., DuBois, P., & Blankenhorn, G. (2018b). Implementation of deformation, damage, and failure in an orthotropic plasticity material model, manuscript in progress

Toray Composite Materials America, Inc. (2017). <https://www.toraycma.com/>